nature geoscience

LETTERS

PUBLISHED ONLINE: 14 OCTOBER 2012 | DOI: 10.1038/NGEO1601

Direct measurement of hydroxyl in the lunar regolith and the origin of lunar surface water

Yang Liu[1]*, Yunbin Guan[2], Youxue Zhang[3], George R. Rossman[2], John M. Eiler[2] and Lawrence A. Taylor[1]

Remote sensing discoveries of hydroxyl and water on the lunar surface have reshaped our view of the distribution of water and related compounds on airless bodies such as the Moon[1–3]. The origin of this surface water is unclear[4], but it has been suggested that hydroxyl in the lunar regolith can result from the implantation of hydrogen ions by the solar wind[1,5]. Here we present Fourier transform infrared spectroscopy and secondary ion mass spectrometry analyses of Apollo samples that reveal the presence of significant amounts of hydroxyl in glasses formed in the lunar regolith by micrometeorite impacts. Hydrogen isotope compositions of these glasses suggest that some of the observed hydroxyl is derived from solar wind sources. Our findings imply that ice in polar cold traps could contain hydrogen atoms ultimately derived from the solar wind, as predicted by early theoretical models of water stability on the lunar surface[6]. We suggest that a similar mechanism may contribute to hydroxyl on the surfaces of other airless terrestrial bodies where the solar wind directly interacts with the surface, such as Mercury and the asteroid 4-Vesta.

The past few years have witnessed a paradigm shift in our view of 'no water' on the Moon. This revolution started with the report of significant H in lunar volcanic glasses[7] and was followed by finds of high H contents of lunar apatite[8–10] and melt inclusions[11]. These measurements were made by secondary ion mass spectrometry (SIMS), which cannot distinguish H species, but the measured H was suggested to be most likely OH. Equally important are the discoveries of OH/H_2O in the top millimetres of the lunar regolith, as revealed by reflectance spectra[1–3], which can distinguish various forms of H. Subsequently, the National Aeronautics and Space Administration (NASA) Lunar Crater Observation and Sensing Satellite (LCROSS) mission delivered an impactor into a permanently shadowed lunar crater and observed the resulting plume. Results are consistent with the presence of H_2O ice in cold traps at the lunar poles[12] and support observations of hydrogen by Lunar Prospector's neutron spectrometer[13]. Despite these discoveries of $H/OH/H_2O$ on the Moon, there has been no direct proof of OH/H_2O in specific lunar regolith phases. Although measurements on bulk samples of the lunar regolith have demonstrated the presence of solar-wind H, C, N and noble gases[14], it is unknown whether the solar-wind H was bounded as OH or H_2O (or is present in some other less common form). As a result, the contribution of solar-wind protons to polar ice is debated[13,15]. Answers to these debates are important to understanding the development of the lunar regolith and space weathering on other airless bodies in the solar system (for example, 4-Vesta, Mercury).

Lunar regolith typically refers to all the crushed materials that cover the lunar surface, whereas lunar soils refer to the fraction of particles <1 cm in size. The lunar regolith is produced by space weathering, a term referring to physical and chemical alteration caused by meteorite and micro-meteorite (<1 mm in size) impacts, solar-wind, solar-flare and galactic-cosmic-ray particle bombardments. For the past 3 billion years, micro-meteorite impacts have been the main mechanism altering the regolith by comminution, melting, and vaporization. The solar wind consists of low-energy particles ($\sim$1 keV amu^{-1}, mainly H^+) and only affects the top micrometre of exposed grains by sputtering and implantation[16]. Higher-energy particles in solar-flare and galactic-cosmic rays (1 MeV amu^{-1} to 10 GeV amu^{-1}) penetrate to centimetre to metre depth and cause nuclear reactions in the lunar regolith. The OH observed in the lunar regolith by reflectance infrared was ascribed to neutralized solar-wind protons in the top 50–100 nm of soil grains (or solar-wind implantation)[1,2,4]. Recent irradiation experiments using $\sim$1 keV H^+ and D^+ produced OH and OD on the outer surfaces of lunar soils, proving the feasibility of solar-wind implantation[5].

Agglutinates are unique products of space weathering in the lunar regolith. They are collections of regolith grains cemented by quenched melts (hereafter referred to as agglutinitic glasses) generated by micro-meteorite impacts into the solar-wind-rich regolith. The agglutinitic glasses are vesicle-rich and contain metallic iron particles from nm to μm size. It has been postulated that solar-wind-induced OH may be transferred from grain surfaces into lunar agglutinitic glasses[17]. However, former searches for this hydrogen using infrared spectroscopy have provided inconclusive results[18,19]. Here, we re-examine agglutinitic glasses with Fourier transform infrared spectroscopy (FTIR) and SIMS. Combined, these two methods determine the chemical form of H, its abundances and its isotopic compositions, with a high spatial resolution.

We selected individual grains from Apollo 11 mare soil 10084, Apollo 16 highland soil 64501, and Apollo 17 mare soil 70051. The grains include agglutinates and impact glasses. They were doubly polished and measured for abundance of OH and H_2O using FTIR. These grains, and further singly polished agglutinate grains, were embedded in an indium disc and then analysed using SIMS. The abundances, regardless of the chemical form of H, are expressed as parts per million H_2O by weight (ppmw H_2O) by convention. The hydrogen isotope compositions of these samples were also determined by SIMS to fingerprint the possible sources of H.

Five polished agglutinates from lunar soils 10084 and 70051 exhibit noticeable FTIR absorption in the 3,500–3,125 cm^{-1} range, typical for OH groups (Fig. 1). The estimated OH contents from

[1]Planetary Geosciences Institute, Department of Earth and Planetary Sciences, University of Tennessee, Knoxville, Tennessee 37996, USA, [2]Division of Geological and Planetary Sciences, California Institute of Technology, Pasadena, California 91125, USA, [3]Department of Earth and Environmental Sciences, University of Michigan, Ann Arbor, Michigan 48109, USA. *e-mail: yangl@utk.edu.

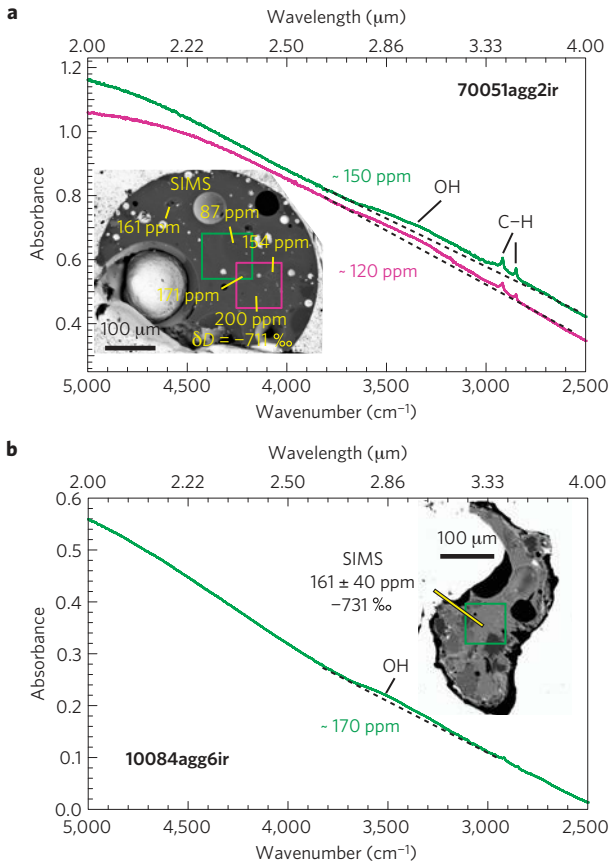

Figure 1 | FTIR spectra and SIMS data of two agglutinates. Each coloured square box on a sample corresponds to a spectrum of the same color. The dashed lines are the linear fit of the continuum (background) of the spectrum. Concentration estimates using FTIR absorbance are labelled next to the spectra. The sharp absorption peaks at ~2,900 cm^{-1} for C-H bands are possibly organic contamination attached to exposed vesicle walls, although it cannot be ruled out that the C-H bands represent genuine lunar signatures. The 2σ uncertainties for SIMS H contents and D/H compositions are estimated based on repeated analyses of standards, fitting errors and counting statistics. Samples come from Apollo 17 soil 70051 (**a**) and Apollo 11 soil 10084 (**b**).

FTIR spectra range from 70 to 170 ppmw H_2O, with uncertainties up to 30% relative (Supplementary Information). The SIMS analyses of these five samples exhibit H abundances equivalent to 160–200 ppmw H_2O, consistent with the FTIR data (Fig. 1 and Supplementary Table S1). The similarity of results using these two methods suggests almost all of the H in the agglutinates analysed by SIMS is in the form of OH. Other forms, such as H_2 or C–H species, if present at all, are apparently minor.

SIMS results of 13 agglutinates indicate that the agglutinitic glasses contain H equivalent to 27 ± 14 to 470 ± 18 ppmw H_2O (Fig. 2 and Supplementary Table S1). Mineral fragments (plagioclase and pyroxene) in these agglutinates contain trace amounts of H that are similar to or slightly above that measured in a nominally anhydrous standard (<1 ppmw H_2O, Supplementary Information). We also examined impact glasses that are free of vesicles, and sometimes free of inclusions, which were possibly formed by meteorite impacts into rock fragments. These impact glasses are as poor in H as the H-free standard. Our results demonstrate that agglutinitic glasses, not minerals, host the majority of the H in the samples, contain it mostly as OH, and that only those glasses formed from soil precursors (as opposed to rock fragments) contain this H. For 21 analyses on Apollo 10084 agglutinitic glasses, the mean- and median-OH contents are similar, 177 versus 174 ppmw H_2O respectively. Using the mean value, and the amount of agglutinitic glasses in the bulk soil (~40 wt%; ref. 20), our data suggest ~70 ppmw H_2O in soil sample 10084, lower than earlier reports of $9.5–25.4 \times 10^{-6}$ mol H_2 g^{-1} (171–458 ppmw H_2O) in bulk sample 10084 (ref. 21).

The D/H values of eight agglutinates range from δD_{SMOW} of -844 ± 40‰ to $+4,206 \pm 134$‰ (2SD) (Fig. 2). The majority of our data (6 agglutinates) lie below δD of −550‰. Two agglutinates (10084agg2; 10084agg8ir) exhibit positive δD values ($+191 \pm 99$‰ to $4,206 \pm 134$‰). The H isotope compositions of these agglutinates significantly differ from the visible contaminants in vesicles and cracks with δD of about −50 to −200‰. On this basis, we infer that the measured D/H compositions of lunar agglutinates largely reflect components intrinsic to the returned lunar soils, rather than terrestrial contamination. Furthermore, if terrestrial contamination produced the observed OH, we would expect D/H values and 1/H follow a mixing line between the Earth and solar wind. Such a trend is not evident in Fig. 3.

Three sources have been suggested for OH in the lunar regolith, including redistribution of implanted solar-wind hydrogen[1–3], trapped volcanic gas[11], and redistribution of H introduced to the lunar surface through comet or meteor impacts[3,12,13]. Hydrogen isotope ratios potentially discriminate among these sources. The incorporation and reworking of implanted OH into the agglutinitic glasses through impact melting could have increased the D/H values because H diffuses more rapidly than D. However, agglutinitic glasses are apparently very heterogeneous in D/H ratio at the scale of individual samples. This implies they never spent significant time hot and molten, or the H isotopes would have homogenized by diffusion. Rather, they must be products of very brief flash heating and immediate quenching back to glass.

The present-day solar wind is highly depleted in D ($D/H < 10^{-7}$ or $\delta D \approx -1{,}000$‰; ref. 22), which is much lower than all agglutinates analysed in this study. Nevertheless, all other plausible sources of H are significantly higher in D/H ratio than we measure in most agglutinate glasses, so our data strongly suggest that a large fraction (perhaps half or more) of the H we observe is ultimately derived from solar-wind protons. It is possible that D in these samples was generated by cosmic-ray spallation[21]. A simple calculation suggests D in five agglutinates we analysed can be explained by spallation generation (details in the Supplementary Information). The most important implication of our results is that hydrogen can be implanted into lunar soils from the solar wind and subsequently transferred to agglutinitic glass through micrometeorite gardening and melting of solar-wind-rich soils.

Three grains of Apollo 11 soil 10084 (10084agg2, 10084agg3, 10084agg8ir) seem to contain too much D to be the result of spallation alone. If D in these grains were all derived from spallation, their exposure ages would be 0.6 Gyr (10084agg3), 1.3–1.5 Gyr (10084agg8ir) and 14 Gyr (10084agg2) assuming the same D production rate (Supplementary Information). Considering the poorly constrained production rate, the lower end of this range is possible, but the upper end is not. Thus, either production rates of D through spallation are strongly underestimated in prior studies, or grain 10084agg2 contains D from some other source.

Although solar wind and spallation seem capable of explaining the sources of H in most agglutinates, we consider several alternative hypotheses. If the measured H in agglutinates is trapped volcanic gas, we expect it should be in equilibrium with that remaining in volcanic glass beads. The δD values for volcanic glass beads were previously measured to be +340‰ for the most volatile rich sample[23]. The hydrogen isotope composition of the vapour in equilibrium with such melts is $\delta D \approx +280$ to +330‰ (Supplementary Information). Trapping of such vapour obviously

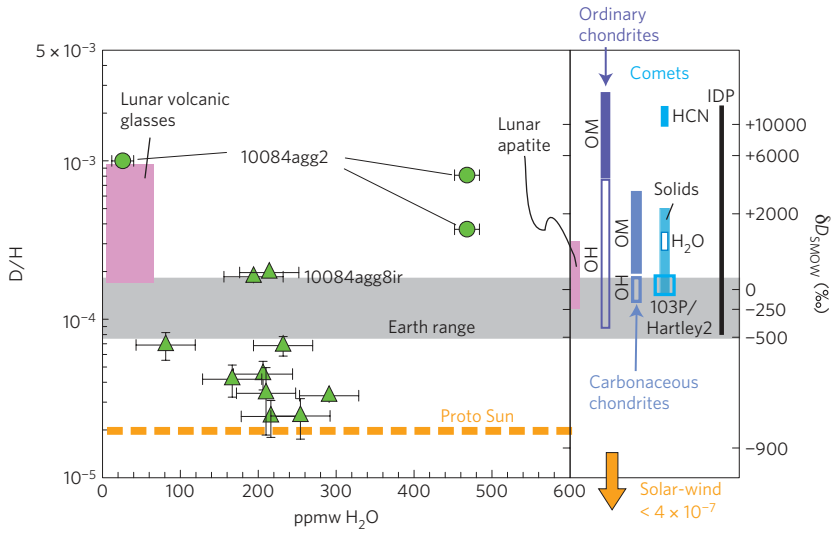

Figure 2 | D/H values versus OH contents (in ppmw H_2O) of lunar agglutinitic glasses. D/H is corrected for IMF and OH is calculated after subtracting background values. $\delta D_{SMOW}(‰) = [(D/H)_{measured}/(D/H)_{standard} - 1] \times 1{,}000$, where the standard is Vienna Standard Mean Ocean Water (SMOW) with D/H of 1.5576×10^{-4}. Error bars (2σ) are shown if they are larger than the symbol size. The D/H values from other planetary sources are plotted for comparison including present-day solar-wind[22], the proto Sun, Earth, comets and chondrites[27,28], interplanetary dust particles[29,30] (IDP) and lunar apatite[10] and glasses[23]. OM, organic matter.

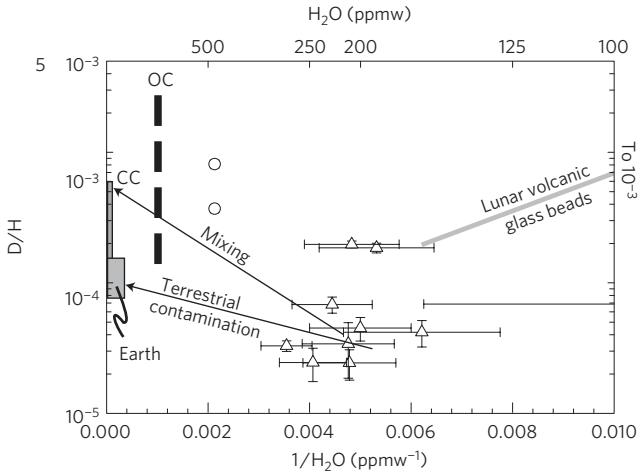

Figure 3 | The D/H values of agglutinates versus $1/H_2O$ contents. Symbols for agglutinate glasses are the same as in Fig. 2. Error bars (2σ) are shown if they are larger than the symbol size. Data of Earth[27], carbonaceous chondrites[27] (CC), ordinary chondrites[27] (OC) and those of volcanic glass[23] are plotted for comparison. Arrowed lines show the possible mixing trends. One point of 10084agg2 (27 ppmw H_2O) is off the scale in this figure.

could not explain the majority of agglutinates with $\delta D < -500‰$, but might contribute, directly or indirectly, to the higher overall D content of 10084agg2.

If OH in the lunar agglutinates is ultimately derived from meteoritic impactors, it should be similar in D/H ratio to known cometary and meteoritic materials. Because some meteorites and comets have δD values higher than 5,400‰ (Fig. 2), they provide a viable source for the very high δD values in the agglutinate 10084agg2 observed in this study. Although it is suspected that addition of H (in some form) from cometary and meteoritic impacts dominated the formation of ice in the permanently shadowed regions of the Moon[13], our study provides the first evidence that such a source could contribute to at least some components of the lunar regolith.

Overall, the hydrogen isotope compositions show that OH in lunar agglutinates is derived from solar-wind protons, but is either modified by subsequent fractionation or admixed with another non-solar-wind source. This conclusion is consistent with mixing between solar-wind and non-solar-wind sources, observed from nitrogen and noble-gas isotope compositions of lunar soils[24]. The majority of agglutinates investigated in this study contains OH derived from solar wind, somewhat more than the 50% to 30% contribution suggested by nitrogen isotopes for Luna 24 soils[24]. This difference could reflect different efficiencies of trapping solar-wind H and N, or different retention rates for different exposure ages (100 Myr for Apollo 10084 versus 500 Myr for Luna 24), or hydrogen isotope fractionation that preferentially elevates the D/H ratio of the component trapped in agglutinates.

Our study identified a new reservoir of OH on the Moon, in addition to those recognized in previous studies of magmatic glasses and apatites. Because agglutinates make up a major proportion of lunar soils, often reaching 50 vol% of a mature soil[20,25], the detected OH in agglutinates represents an unanticipated, abundant reservoir of OH/H_2O in lunar regolith. The exposure age of a soil at the lunar surface is proportional to its agglutinate content[25]. Therefore, our results indicate that older lunar soils might contain higher OH than younger lunar soils.

Lunar soils used in this study were all collected in the equatorial region of the near side of the Moon, where the solar-wind fluence is smaller than other regions and the degassing rate is faster[14,26]. The retention of solar-wind-produced OH in these samples supports solar-wind as a viable source for water-ice in polar cold-traps. Confirmation of a solar-wind and a non-solar-wind source for OH in agglutinates provides further information about the formation of surface OH/H_2O on other airless bodies, such as Mercury and 4 Vesta.

Methods

Analytical methods. Sample and full methods can be found in the Supplementary Information. Transmitted infrared spectra were collected on the doubly-polished grains using a Perkin–Elmer Spectrum FTIR GX microscope at the University of Michigan. The OH content can be estimated using the 3,500-cm^{-1} band-intensity, relative to the continuum-baseline (Fig. 1). These estimates show large uncertainties, mostly because of the small peaks, which introduce difficulty in subtracting a sloping baseline, but also because of uncertainties in sample thickness

and in absorption coefficient. As a result of these factors, the uncertainty in the estimated OH contents is 20–30% relative.

Agglutinates used for FTIR analyses as well as further ones were then imaged and analysed with a Cameca SX-100 Electron Microprobe at the University of Tennessee. Back scattered electron (BSE) images were collected on these agglutinates. The compositions of the glass and minerals were acquired with the following analytical conditions, including a voltage of 15 keV, a current of 10 nA, and 5–10 μm diameter beam. Natural and synthetic standards were used for calibration and measured periodically within analytical sessions to ensure optimum data quality. Detection limits are typically <0.05 wt% for SiO_2, Al_2O_3, MgO, CaO, Na_2O, K_2O and P_2O_5; 0.06–0.1 wt% for FeO, TiO_2, SO_2 and P_2O_5.

Analyses for H abundances and D/H values were conducted in two sessions with a Cameca IMS-7f GEO ion probe at Caltech. For both sessions, the areas of interest were examined carefully using ion imaging to avoid C and H hotspots (cracks, vesicles). Spots chosen for SIMS analyses are near Electron Microprobe measurement points. Following a ~3 min sputtering, glassy regions were measured for 20 cycles through the mass sequence of $^{12}C^-$, $^{16}O^1H^-$, $[^{18}O^-]$, $^{12}C^{16}N^-$, $^{30}Si^-$, $[^{31}P^-]$, $^{32}S^-$, and $^{35}Cl^-$, where the masses in brackets were only measured in the second session. A mass resolving power ($M/\Delta M$) of 5,500 was used to separate the $^{16}O^1H$ peak from ^{17}O. The 2σ uncertainties (Supplementary Table S1) of the H measurements were estimated based on the external errors of the standards (repeated measurements of the standards, the errors associated with them, both in their slopes and intercepts) and the internal errors.

D/H measurements were conducted on the same spots where H abundances were obtained. The mass sequence of $^1H^-$, $^2H^-$, and $^{16}O^-$ was measured for 15–20 cycles each with 1, 15 and 1 s counting times. The analyses of the rhyolitic glass yielded an instrument mass fractionation (IMF) of +30‰. All reported values were corrected for the IMF. The 4σ uncertainties (Fig. 2 and Supplementary Table S1) include both external errors (repeated analyses of the rhyolitic standard) and internal errors (counting statistics).

Received 1 May 2012; accepted 12 September 2012; published online 14 October 2012

References

1. Pieters, C. M. *et al.* Character and spatial distribution of OH/H_2O on the surface of the Moon seen by M3 on Chandrayaan-1. *Science* **326,** 568–572 (2009).
2. Sunshine, J. M. *et al.* Temporal and spatial variability of lunar hydration as observed by the deep impact spacecraft. *Science* **326,** 565–568 (2009).
3. Clark, R. N. Detection of adsorbed water and hydroxyl on the Moon. *Science* **326,** 562–564 (2009).
4. McCord, T. B. *et al.* Sources and physical processes responsible for OH/H_2O in the lunar soil as revealed by the Moon mineralogy mapper (M3). *J. Geophys. Res.* **116,** E00G05 (2011).
5. Ichimura, A. I., Zent, A. P., Quinn, R. C., Sanchez, M. R. & Taylor, L. A. Hydroxyl (OH) production on all airless planetary bodies: Evidence from H^+/D^+ ion-beam experiments. *Earth Planet. Sci. Lett.* **345,** 90–94 (2012).
6. Watson, K., Murray, B. C. & Brown, H. The behavior of volatiles on the lunar surface. *J. Geophys. Res.* **66,** 3033–3045 (1961).
7. Saal, A. E. *et al.* Volatile content of lunar volcanic glasses and the presence of water in the Moon's interior. *Nature* **454,** 192–196 (2008).
8. Boyce, J. W. *et al.* Lunar apatite with terrestrial volatile abundances. *Nature* **466,** 466–469 (2010).
9. McCubbin, F. M. *et al.* Nominally hydrous magmatism on the Moon. *Proc. Natl Acad. Sci. USA* **107,** 11223–11228 (2010).
10. Greenwood, J. P. *et al.* Hydrogen isotope ratios in lunar rocks indicate delivery of cometary water to the Moon. *Nature Geosci.* **4,** 79–82 (2011).
11. Hauri, E. H., Weinreich, T., Saal, A. E., Rutherford, M. C. & Van Orman, J. A. High pre-eruptive water contents preserved in lunar melt inclusions. *Science* **333,** 213–215 (2011).
12. Colaprete, A. *et al.* Detection of water in the LCROSS ejecta plume. *Science* **330,** 463–468 (2010).
13. Feldman, W. C. *et al.* Evidence for water ice near the lunar poles. *J. Geophys. Res.* **106,** 23231–23251 (2001).
14. Fegley, B. Jr & Swindle, T. D. *Resources of Near-Earth Space* 367–426 (1993).
15. Hiroi, T., Pieters, C. M. & Takeda, H. Grain size of the surface regolith of Asteroid 4 Vesta estimated from its reflectance spectrum in comparison with HED meteorites. *Meteoritics* **29,** 394–396 (1994).
16. Keller, L. P. & McKay, D. S. The nature and origin of rims on lunar soil grains. *Geochim. Cosmochim. Acta* **61,** 2331–2341 (1997).
17. Crider, D. H. & Vondrak, R. R. The solar wind as a possible source of lunar polar hydrogen deposits. *J. Geophys. Res.* **105,** 26773–26782 (2000).
18. Taylor, L. A., Rossman, G. R. & Qu, Q. Where has all the lunar water gone? *Lunar Planet. Sci. Conf.* **26,** abstr. 1399 (1995).
19. McKay, D. S. *et al.* Apollo 16 regolith breccias: Characterization and evidence for early formation in the mega-regolith. *J. Geophys. Res.* **91,** D277–D303 (1986).
20. Taylor, L. A., Pieters, C. M., Keller, L. P., Morris, R. V. & McKay, D. S. Lunar mare soils: Space weathering and the major effects of surface-correlated nanophase Fe. *J. Geophys. Res.* **106,** 27985–27999 (2001).
21. Epstein, S. & Taylor, H. P. O^{18}/O^{16}, Si^{30}/Si^{28}, D/H, and C^{13}/C^{12} ratios in lunar samples. *Proc. 2nd Lunar Sci. Conf.* **2,** 1421–1441 (1971).
22. Huss, G. R., Nagashima, K., Burnett, D. S., Jurewicz, A. J. G. & Olinger, C. T. A new upper limit on the D/H ratio in the solar wind. *Lunar Planet. Sci. Conf.* **43,** abstr. 1709 (2012).
23. Saal, A. E., Hauri, E. H., Van Orman, J. A. & Rutherford, M. C. D/H ratios of the lunar volcanic glasses. *Lunar Planet. Sci. Conf.* **43,** abstr. 1327 (2012).
24. Füri, E., Marty, B. & Assonov, S. S. Constraints on the flux of meteoritic and cometary water on the Moon from volatile element (N–Ar) analyses of single lunar soil grains, Luna 24 core. *Icarus* **218,** 220–229 (2012).
25. McKay, D. S. *et al.* in *Lunar Sourcebook* (eds Heiken, G., Vaniman, D. & French, B.) (Cambridge Univ. Press, 1991).
26. Starukhina, L. Water detection on atmosphereless celestial bodies: Alternative explanations of the observations. *J. Geophys. Res.* **106,** 14701–14710 (2001).
27. Robert, F., Gautier, D. & Dubrulle, B. The solar system D/H ratio: Observations and theories. *Space Sci. Rev.* **92,** 201–224 (2000).
28. Hartogh, P *et al.* Ocean-like water in the Jupiter-family comet 103P/Hartley 2. *Nature* **478,** 218–220 (2011).
29. Gopalan, K., Goswami, J. N., Rao, M. N., Suthar, K. M. & Venkatesan, T. R. Solar cosmic ray produced noble gases and tracks in lunar fines 10084 and 14163. *Proc. Lunar Sci. Conf.* **8,** 793–811 (1977).
30. Housley, R. M., Grant, R. W. & Paton, N. E. Origin and characteristics of excess Fe metal in lunar glass welded aggregates. *Geochim. Cosmochim. Acta* **3** (Proc. 4th Lunar Sci. Conf., Suppl. 4), 2737–2749 (1973).

Acknowledgements

This work is supported in part by NASA Cosmochemistry grants NNX11AG58G (L.A.T.), NNX10AH74G (Y.Z.), the support from the Moore Foundation to the Caltech Microanalysis Center (J.M.E.), and NSF grant EAR-0947956 (G.R.R.). A portion of this study was also supported by the Planetary Geosciences Institute at UTK. We thank Z. Xu for her assistance with FTIR analyses at UM, M. L. Voyer for kindly providing glass standards, and J. Mosenfelder for providing the dry olivine standard.

Author contributions

Y.L. led the project from the sample preparation, the FTIR and SIMS measurements, to the paper writing. Y.G. set up the SIMS instrument and assisted in the formulation of the analytical protocol. Y.Z. assisted in the infrared analyses for all agglutinates. G.R.R. assisted in the preliminary infrared analyses of three agglutinates. L.A.T. initialized the search for water in agglutinates with G.R.R. ~20 yr ago, has championed this endeavor since, and was allocated the lunar soil samples by NASA. All authors participated in the data interpretation and paper writing.

Additional information

Supplementary information is available in the online version of the paper. Reprints and permissions information is available online at www.nature.com/reprints. Correspondence and requests for materials should be addressed to Y.L.

Competing financial interests

The authors declare no competing financial interests.

nature geoscience

SUPPLEMENTARY INFORMATION

DOI: 10.1038/NGEO1601

Direct Measurement of Hydroxyl in the Lunar Regolith and the Origin of Lunar Surface Water

Yang Liu[1*], Yunbin Guan[2], Youxue Zhang[3], George R. Rossman[2], John M. Eiler[2], and Lawrence A. Taylor[1]

[1]Planetary Geosciences Institute, Department of Earth & Planetary Sciences, University of Tennessee, Knoxville, TN 37996.
[2]Division of Geological and Planetary Sciences, California Institute of Technology, Pasadena, CA 91125.
[3]Department of Earth and Environmental Sciences, University of Michigan, Ann Arbor, MI 48109.

Supplementary Information

1. Samples

Agglutinates were picked from three soil samples. Apollo 11 soil 10084 is a mature soil, whereas Apollo 16 soil 64501 is a sub-mature one. Sample 70051 was collected from the surface of the lunar rover at the conclusion of the Apollo 17 mission, and is considered to be immature[1].

2. Analytical methods

All reported FTIR data were collected using a microscope of a Perkin-Elmer Spectrum FTIR GX at the University of Michigan. Transmitted IR spectra were collected using a visible source, a CaF_2 beamsplitter, a liquid-N_2 cooled MCT detector, a rectangle aperture (100 by 80-100 μm), 512 scans, resolution of 4 cm^{-1}, and a gain of 1 to 4. To minimize the interference of atmospheric H_2O, samples were shielded in a compartment purged with a constant N_2 flow, and a new background scan was collected just before the sample scan. The total H_2O contents were

estimated following the Beer-Lambert law: $c = 18.02 \times Abs/(d \times \rho \times \varepsilon)$, where *Abs* is the absorbance at ~3480 cm^{-1} (peak value) corrected for the baseline, *d* is the thickness of the sample, ε is the molar absorption coefficient and is 61 *l*/mol/cm for the basaltic glass[2], ρ is the density of the glass assuming a constant value of 3000 kg/m^3. The ε values differ by <6% among different basalts[3]. Detection limit of the FTIR spectrometer is ~10 ppmw H_2O. However, owing to the small size of the peak at ~3500 cm^{-1} and the uncertainty in sample thickness and in the baseline fitting, the estimated OH contents are much larger (20 to 30%).

Back scattered electron (BSE) images and the composition of the glasses and minerals were acquired using a Cameca SX-100 electron microprobe (EMP) at the University of Tennessee. Analytical conditions include a voltage of 15 KeV, a current of 10 nA, and a 10 μm beam diameter. Natural and synthetic minerals are used as standards. Detection limits are typically <0.05 wt% for SiO_2, Al_2O_3, MgO, CaO, Na_2O and K_2O; 0.06-0.1 wt% for FeO, TiO_2, Cr_2O_3, MnO, P_2O_5 and S. Major and minor element contents of glass and minerals are shown in Supplementary Table 1 and Supplementary Figure 1.

Analyses for H abundances and D/H values were conducted in two sessions with a Cameca ims-7f GEO ion probe at Caltech. For both sessions, the areas of interest were examined carefully using ion imaging to avoid C and H hotspots (cracks, vesicles). Spots chosen for SIMS analyses are near EMP points. Following a ~3 min sputtering, glassy regions were measured for 20 cycles through the mass sequence of $^{12}C^-$, $^{16}O^1H^-$, [$^{18}O^-$], $^{12}C^{16}N^-$, $^{30}Si^-$, [$^{31}P^-$], $^{32}S^-$, and $^{35}Cl^-$, where the masses in brackets were only measured in the second session. A mass resolving power (ΔM/M) of 5500 was used to separate the $^{16}O^1H$ peak from ^{17}O. Terrestrial basaltic glasses with 150 and 260 ppmw H_2O[4] were used as standards for H abundances (Supplementary Figure 2). Supplementary Figure 3 shows an example of the SIMS spectra for OH

measurements. The instrument H backgrounds of the two sessions were monitored with a dry olivine standard (GRR1017, <<1 ppmw H_2O[5]). The background $^{16}O^{1}H^{-}/^{30}Si^{-}$ values were subtracted from those of standards and samples. Using the method in Mosenfelder et al.[5], the detection limit of SIMS is estimated to be 7 and 5 ppmw H_2O for two sessions, respectively. The uncertainties (2σ in Supplementary Table 1) of the OH measurements were estimated based on the external errors of the standards (repeated measurements of the standards, the errors associated with them, both in their slopes and intercepts) and the internal errors.

D/H measurements were conducted on the same spots where H abundances were obtained. The mass sequence of $^{1}H^{-}$, $^{2}H^{-}$, and $^{16}O^{-}$ was measured for 15-20 cycles each with 1 s, 15 s and 1 s counting times. One terrestrial rhyolitic glass containing 0.69 wt% H_2O with $\delta D = -69‰_{VSMOW}$ (MC84-df[6]) was used to evaluate the instrument mass fractionation (IMF) of D/H. Given the small OH contents, the matrix effect between basaltic and rhyolitic glasses[7] is insignificant for the results presented in this study. The analyses of the rhyolitic glass yielded an IMF of +30‰. All reported values were corrected for the IMF. The 2σ uncertainties (Fig. 2 and 3, Supplementary Table 1) include both external errors (two analyses of the rhyolitic standard) and internal errors (counting statistics). The analytical spots corresponding to Supplementary Table 1 are shown on the BSE images of the agglutinates (Supplementary Figure 4).

3. Calculation of spallation-generated deuterium

For this calculation, we assume hydrogen was derived from solar-wind and deuterium was generated by cosmic-ray and solar-flare spallation. Using a spallation production rate of D at the surface (1.5×10^{-12} mole D_2/g/Myr)[8], and a solar-flare exposure age of 10084 (100 Ma[9]), we obtained 6×10^{-10} g of spallation-D per gram of the regolith, similar to that estimated by

Epstein and Taylor[10]. The spallation-D (molar) was divided by measured H (molar) in each agglutinates and then compared to measured D/H values (Supplementary Figure 5). Five agglutinates lie on the 1:1 line considering the uncertainties in the calculated D/H values (Supplementary Figure 5). Three grains of Apollo 11 soil 10084 (10084agg2, 10084agg3, 10084agg8ir) appear to contain D higher than that from spallation. If D in these grains were all derived from spallation, their exposure ages would be 0.6 Ga (10084agg3), 1.3-1.5 Ga (10084agg8ir) and 14 Ga (10084agg2) assuming the same D production rate. The spallation production rate is poorly constrained. If we assume the rate is 10 times more than the estimated value, the exposure ages decrease to 60 Ma (10084agg3), 130-150 Ma (10084agg8ir), and 1.4 Ga (10084agg2). The lower end of this range is possible, but the upper end is not. Thus, either production rates of D through spallation are strongly under estimated in prior studies, or grain 10084agg2 contains D from some other source.

4. Calculation hydrogen isotope composition of vapor from volcanic degassing

At the oxygen fugacity of IW-2 to IW, the vapor contains H_2 and H_2O. Let R=D/H and x = $X_{H_{2,v}}$. Thus, for the hydrogen isotope composition of the vapor (v), we have:

$$R_v = (1-x) * R_{H_2O_v} + x * R_{H_{2,v}}$$

$$=(1-x) * R_{H_2O_v} + x / \alpha_{H_2O_v - H_2v} \; R_{H_2O_v}$$

$$= (1-x + x / \alpha_{H_2O_v - H_2v}) \, R_{H_2O_v}.$$

The mole fraction of H_2 in the vapor is approximated by the fugacity ratio of H_2/H_2O (10:1 at log f_{O2} = IW-2 to 1:1 at log f_{O2} = IW)[11]. The fractionation factor $\alpha_{H_2O_v - H_2v}$ is 1.0875 at 1300 °C[12]. For the melt, dissolved H_2 and molecular H_2O are insignificant compared to OH[11]. It is thus reasonable to assume there is no fractionation between H_2 in the vapor and that in the melt, and

H_2 in the melt and OH in the melt. Therefore the exchange reactions between vapor and melt follow:

$$H_2O\ (v) + HDO\ (m) = HDO\ (v) + H_2O\ (m)$$

$$H_2O\ (m) + 2\ OH\ (m) = HDO\ (m) + OH\ (m) + OD\ (m)$$

$$R_{H2Ov}/\ R_{OH,\ melt} = \alpha_{H_2O_v\ -\ H_2O_m} * \alpha_{H_2O_m\ -\ OH_m}$$

Using values for rhyolite[6], $\alpha_{H2Ov\ -\ H2Om} = 0.9857$ and $\alpha_{H_2O_m\ -\ OH_m} = 1.049$, we have $\alpha_{H_2O_v\ -\ melt} = 1.034$. Thus,

$$R_v = (1\text{-}x + x/\alpha_{H_2O_v\ -\ H_2v})\ R_{H_2O_v}$$

$$= (1\text{-}x + x/1.087)*\ R_{OH,\ melt}*1.034$$

For $\delta D_{melt} = +\ 340$ ‰ for glass beads corrected for spallation[13], the δD_v in equilibrium with the melt is ~+284 to +330 ‰ for IW-2 to IW, respectively.

5. Supplementary references

1. Hill, E., Mellin, M. J., Deane, B., Liu, Y. & Taylor, L. A. Apollo sample 70051 and high- and low-Ti lunar soil simulants MLS-1A and JSC-1A: Implications for future lunar exploration. *J. Geophys. Res.* **112**, E02006, doi:10.1029/2006je002767 (2007).
2. Danyushevsky, L. V. *et al.* The H_2O content of basaltic glasses from Southwest Pacific back-arc basins. *Earth Planet. Sci. Lett.* **117**, 347-362 (1993).
3. Mandeville, C. W. *et al.* Determination of molar absorptivities for infrared absorption bands of H_2O in andesitic glasses. *Am. Miner.* **87**, 813-821 (2002).
4. Jochum, K. P. *et al.* MPI-DING reference glasses for in situ microanalysis: New reference values for element concentrations and isotope ratios. *Geochem. Geophys. Geosyst.* **7**, doi:10.1029/2005gc001060 (2006).

5. Mosenfelder, J. L. *et al.* Analysis of hydrogen in olivine by SIMS: Evaluation of standards and protocol. *Am. Mineral.* **96**, 1725-1741 (2011).
6. Newman, S., Epstein, S. & Stolper, E. M. Water, carbon dioxide, and hydrogen isotopes in glasses from the ca. 1340 A.D. eruption of the Mono Craters, California: Constraints on degassing phenomena and initial volatile content. *J. Volcanol. Geotherm. Res.* **35**, 75-96 (1988).
7. Hauri, E. H. *et al.* Matrix effects in hydrogen isotope analysis of silicate glasses by SIMS. *Chem. Geol.* **235**, 352-365 (2006).
8. Merlivat, L., Lelu, M., Nief, G. & Roth, E. Deuterium, hydrogen, and water content of lunar material. *Proc. 5th Lunar Sci. Conf., Suppl. 5, Geochim. Cosmochim. Acta* **2**, 1885-1895 (1974).
9. Gopalan, K., Goswami, J. N., Rao, M. N., Suthar, K. M. & Venkatesan, T. R. Solar cosmic ray produced noble gases and tracks in lunar fines 10084 and 14163. *Proc. Lunar Sci. Conf.,* **8**, 793-811 (1977).
10. Epstein, S. & Taylor, H. P. O^{18}/O^{16}, Si^{30}/Si^{28}, D/H, and C^{13}/C^{12} ratios in lunar samples. *Proc. 2nd Lunar Sci.Conf.* **2**, 1421-1441 (1971).
11. Zhang, Y. "Water" in lunar basalts: The role of molecular hydrogen (H_2), especially in the diffusion of the H component. *Lunar Planet. Sci. Conf.* **42**, 1957 (2011).
12. Richet, P., Bottinga, Y. & Javoy, M. A review of hydrogen, carbon, nitrogen, oxygen, sulphur, and chlorine stable isotope fractionation among gaseous molecules. *Ann. Rev. Earth Planet. Sci.* **5**, 65-110 (1977).
13. Saal, A. E., Hauri, E. H., Van Orman, J. A. & Rutherford, M. C. D/H ratios of the lunar volcanic glasses. *Lunar Planet. Sci. Conf.* **43***,* 1327 (2012).

14. Papike, J. J., Simon, S. B. & Laul, J. C. The lunar regolith - chemistry, mineralogy, and petrology. *Rev. Geophy.* **20**, 761-826 (1982).

15. Taylor, L. A., Pieters, C. M., Keller, L. P., Morris, R. V. & McKay, D. S. Lunar mare soils: Space weathering and the major effects of surface-correlated nanophase fe. *J. Geophys. Res.* **106**, 27985-27999 (2001).

16. Taylor, L. A. *et al.* Mineralogical and chemical characterization of lunar highland soils: Insights into the space weathering of soils on airless bodies. *J. Geophys. Res.* **115**, E02002 (2010).

Supplementary Figures and Table

Supplementary Figure 1. Compositions of agglutinitic glasses in this study. Filled fields represent bulk compositions of lunar soils, and open fields show average compositions of agglutinitic glasses[14-16]. Sample 10084agg2 plots together with other agglutinates.

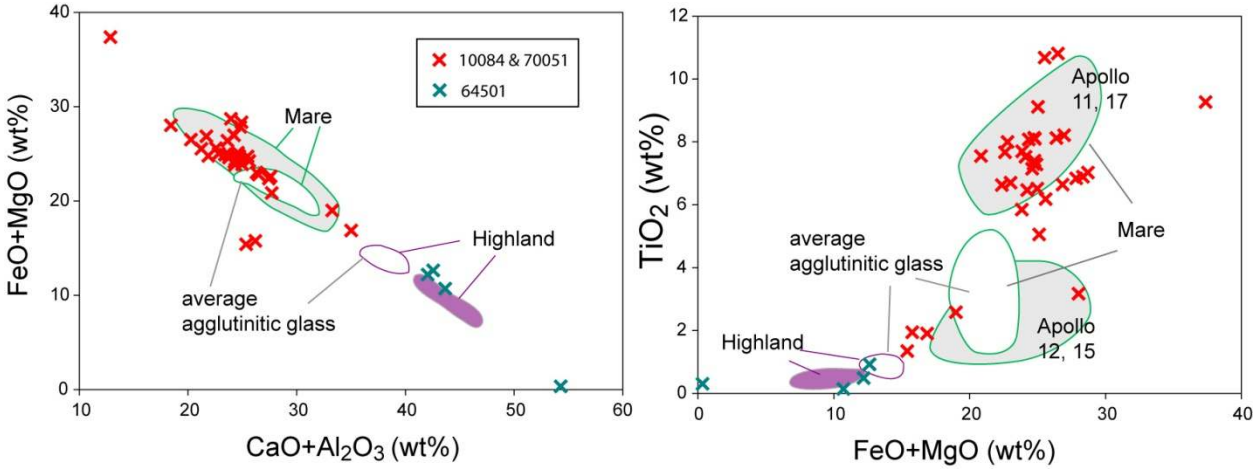

Supplementary Figure 2. Calibration lines for two analytical sessions. The $^{16}O^{1}H/^{30}Si$ values have been background corrected. The 2σ uncertainties of $^{16}O^{1}H/^{30}Si$ and H_2O content are shown if larger than the symbols. Linear regressions were conducted by weighting the $^{16}O^{1}H/^{30}Si$ and H_2O content with their 2σ uncertainties.

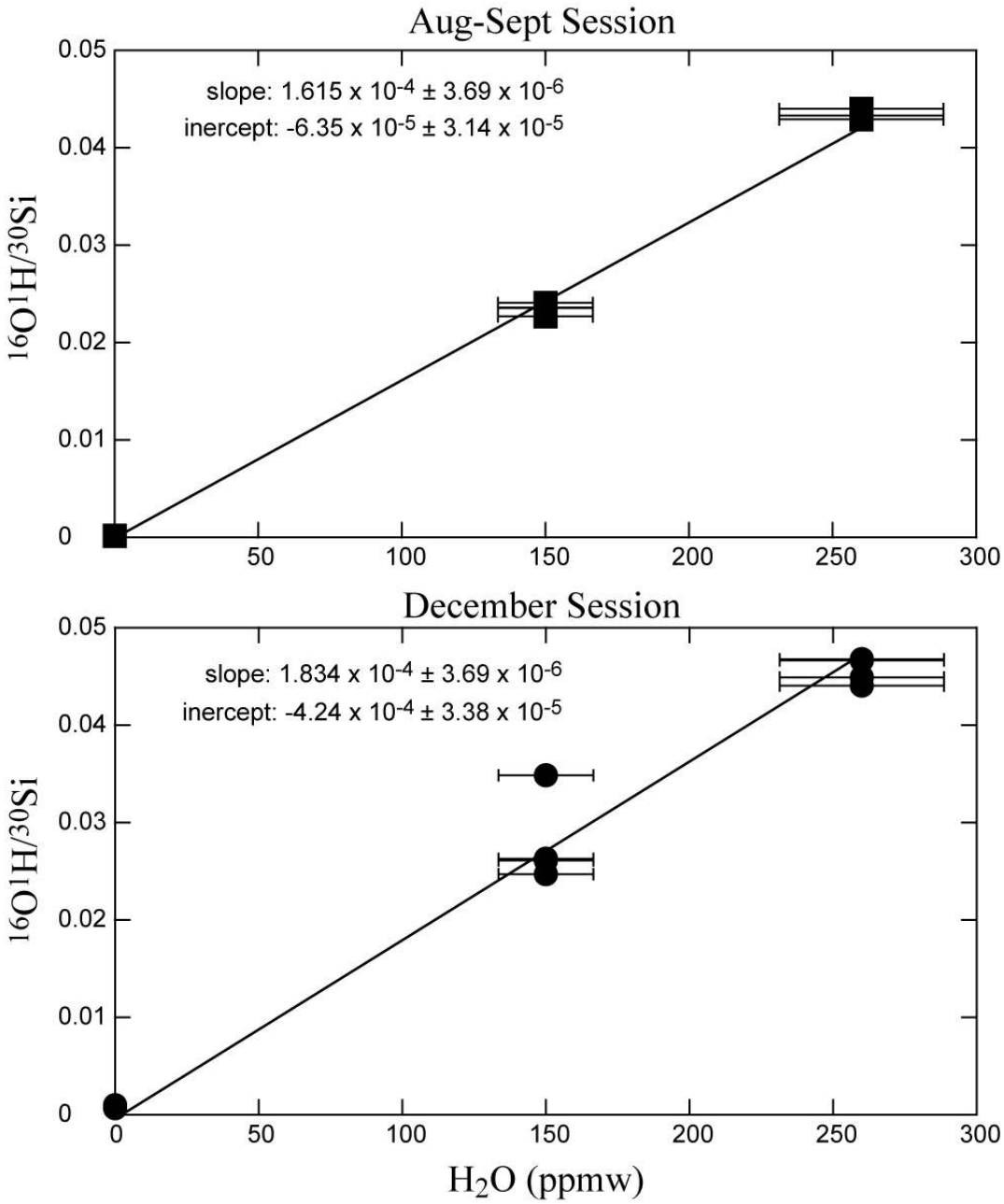

Supplementary Figure 3. SIMS spectrum for OH analysis.

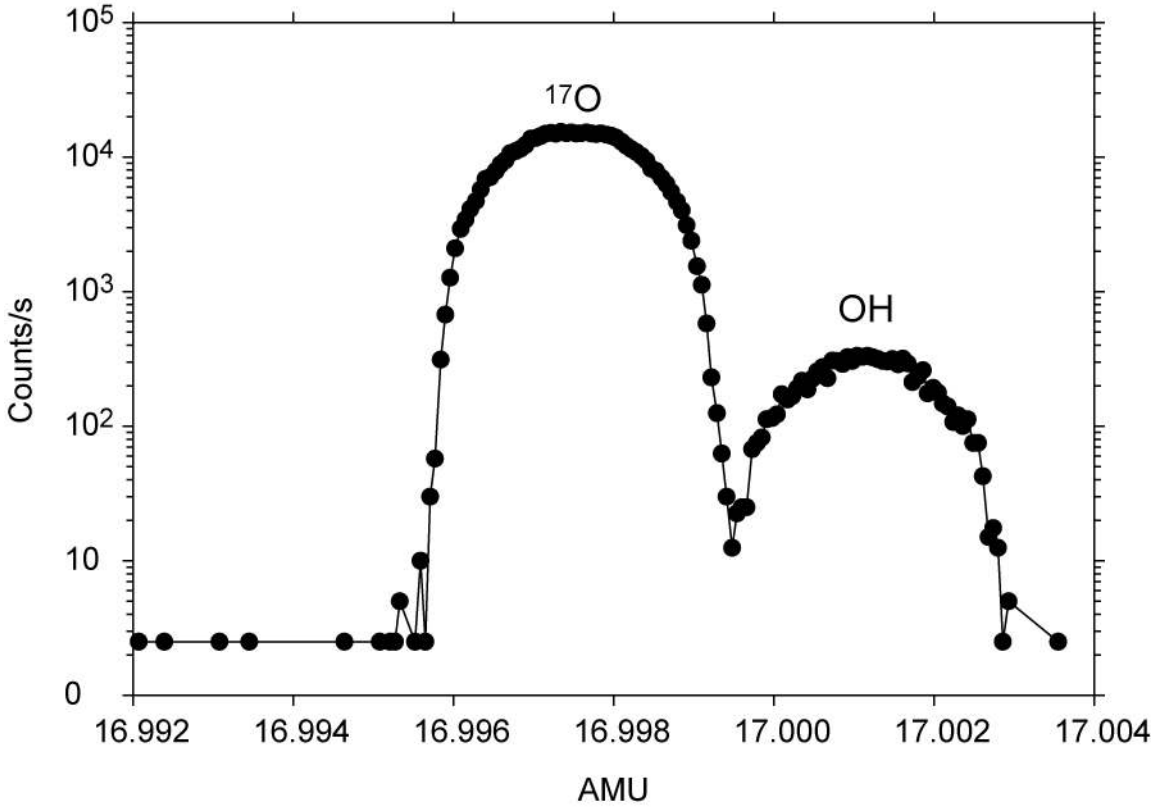

Supplementary Figure 4. Backscattered electron images of lunar agglutinates showing SIMS analytical spots. The SIMS spots for H abundances are labeled according to dates. The spots for D/H ratios are labeled with DH_###. Sample names containing 'ir' indicate that transmitted FTIR analyses had been conducted. Examples of SIMS time-lapsed spectra are plotted for two analyses.

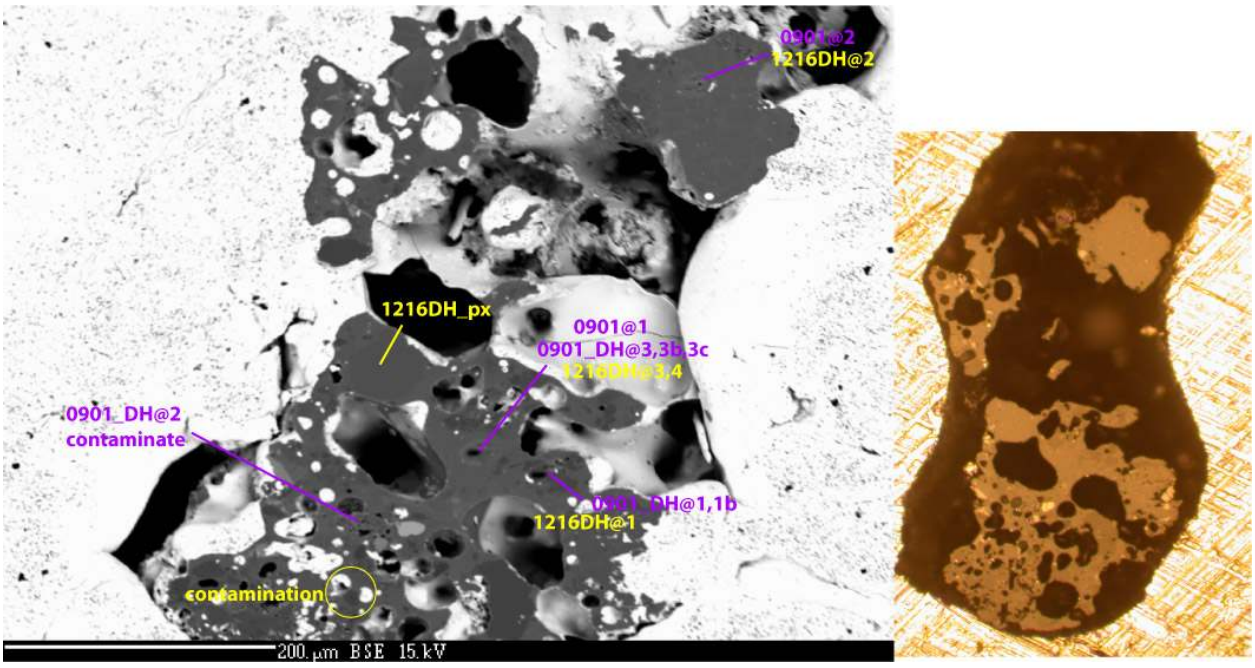

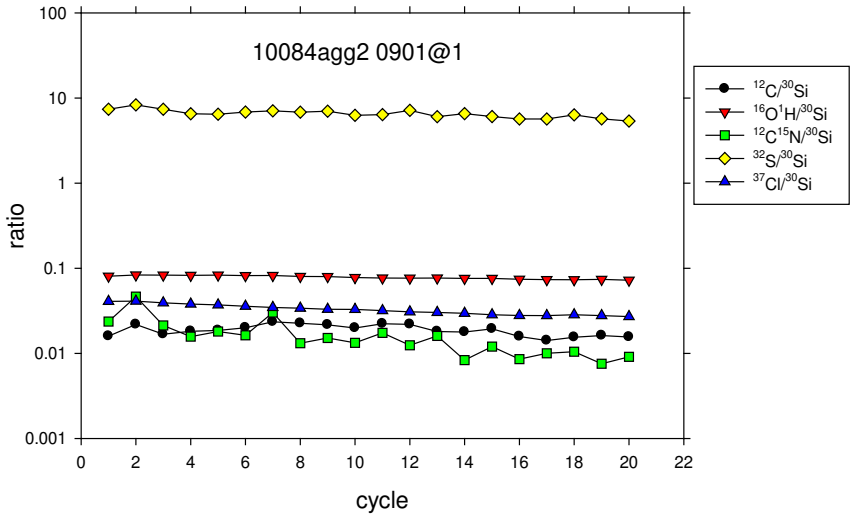

Time lapse plot for spot 0901@1

10084agg2

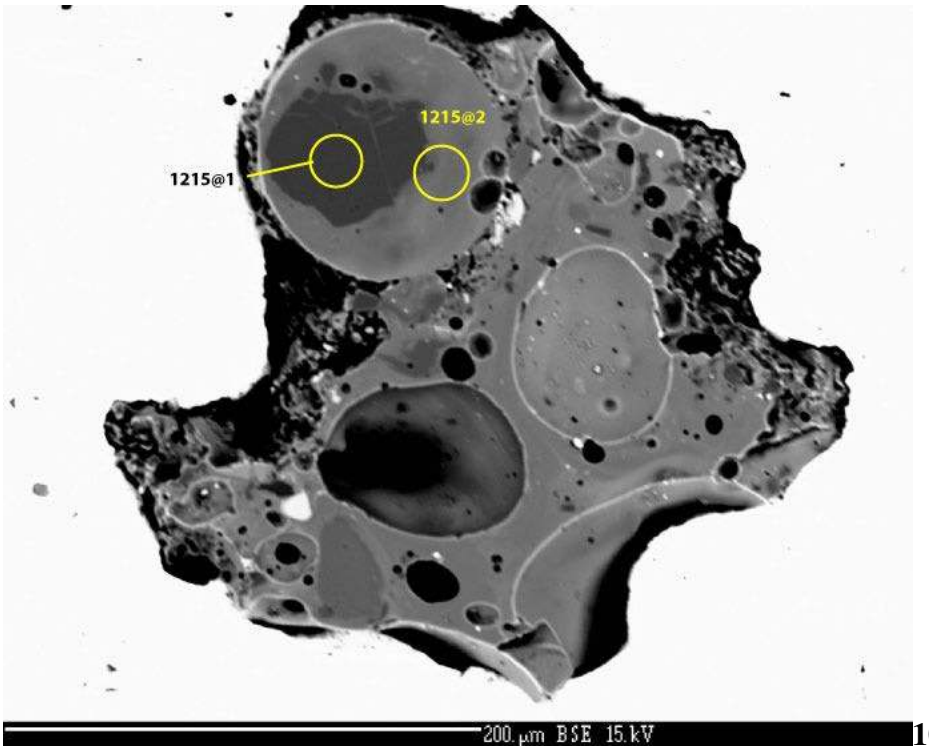

10084 agg1ir

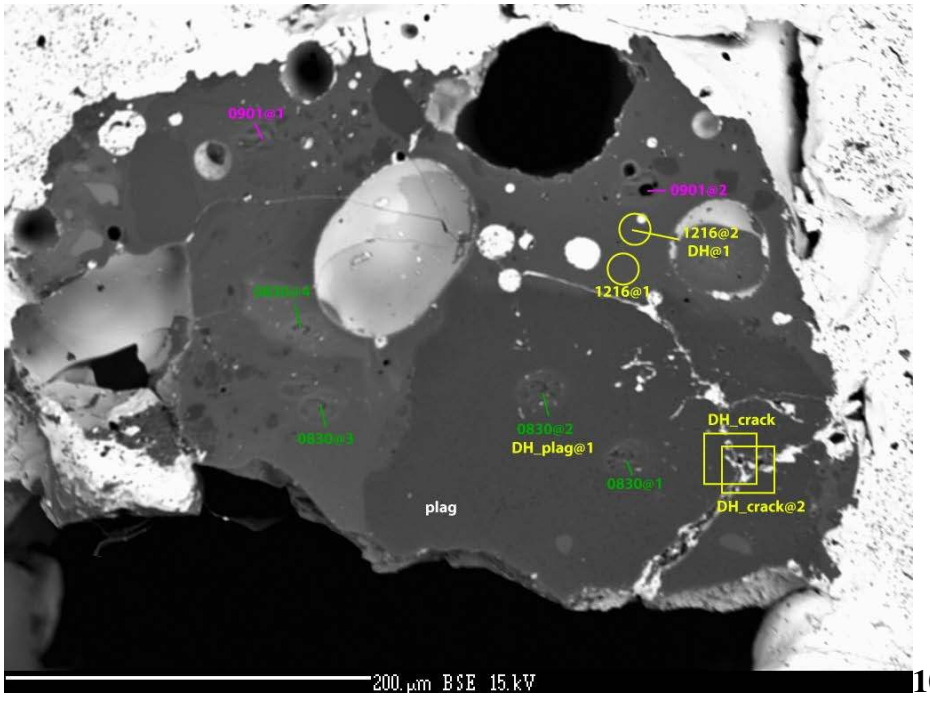

10084agg3

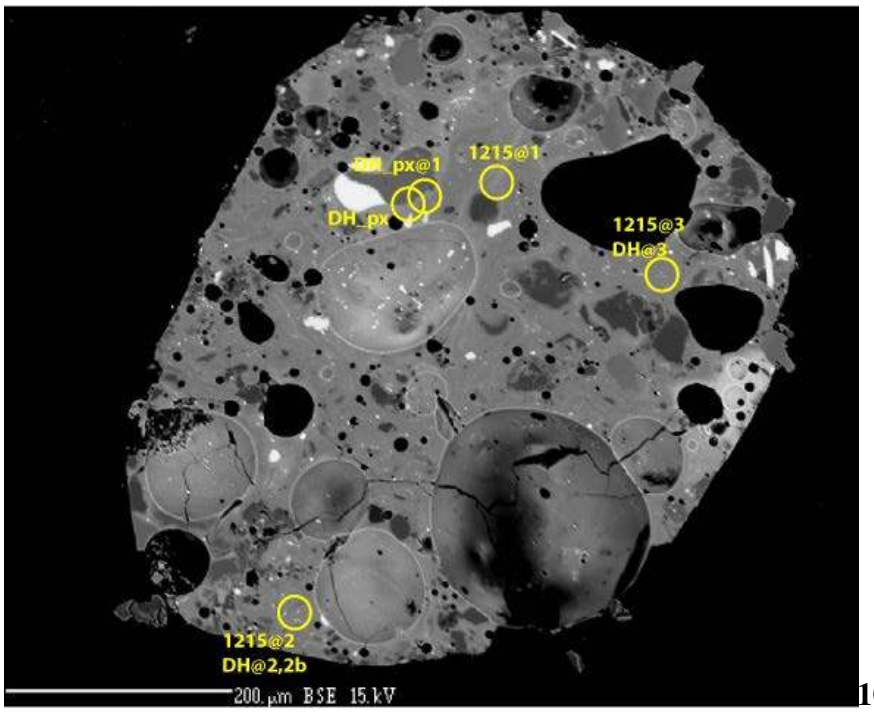

10084agg4n

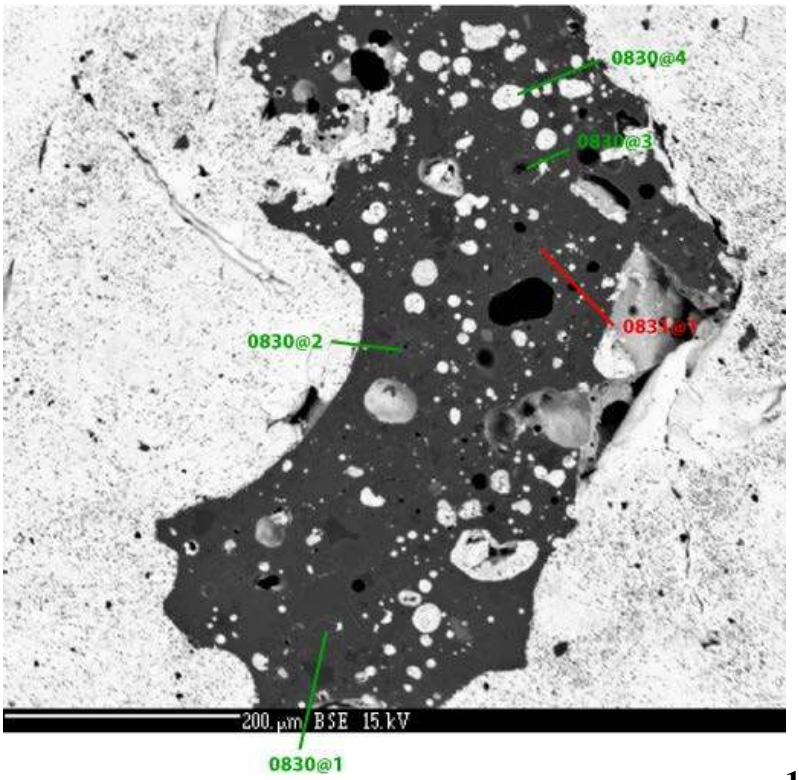

10084 agg5ir

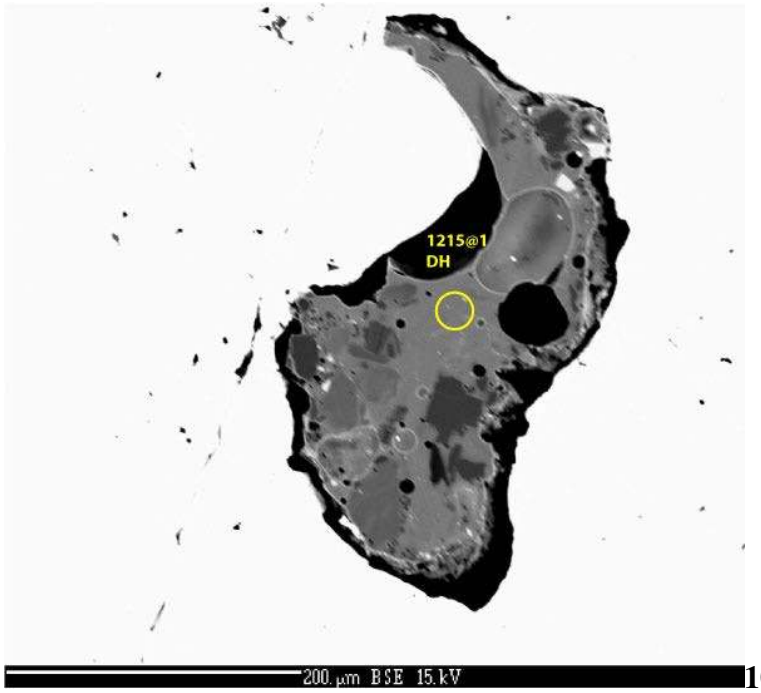

10084agg6ir

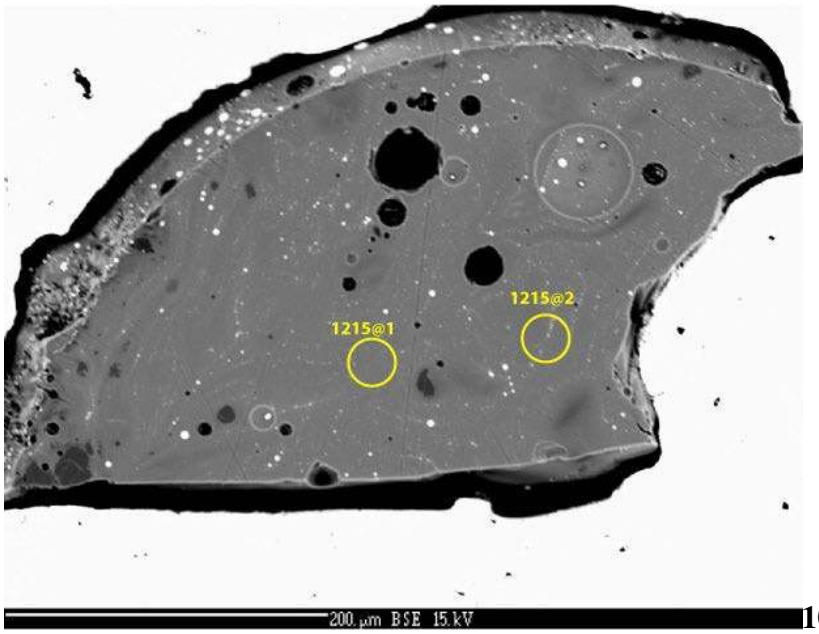

10084 agg7

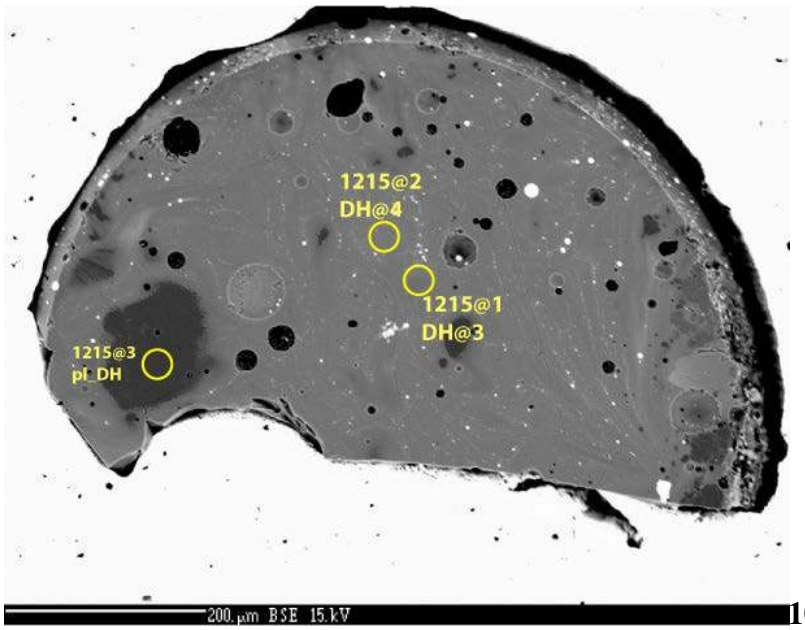

10084 agg8

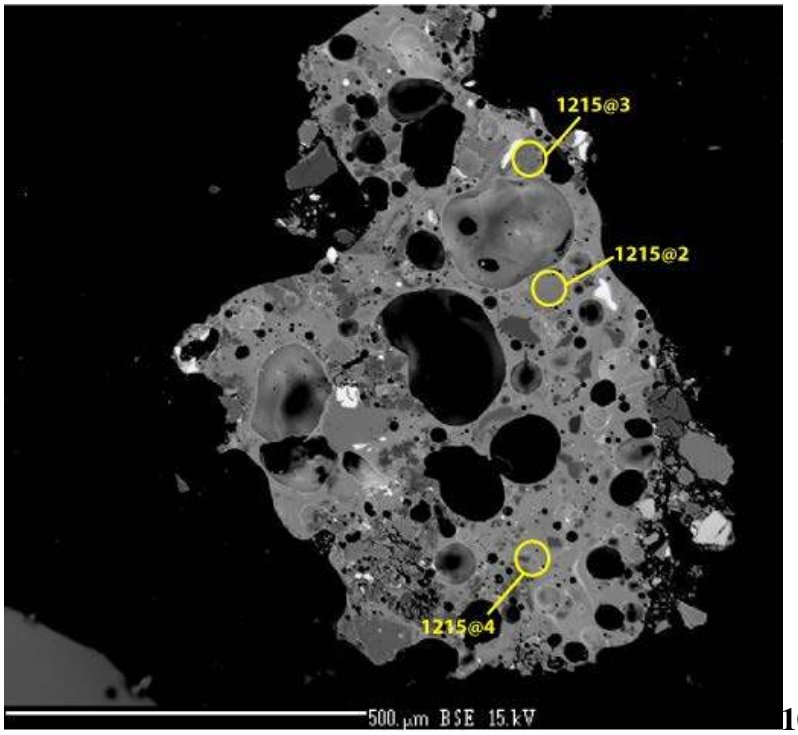

10084 agg9

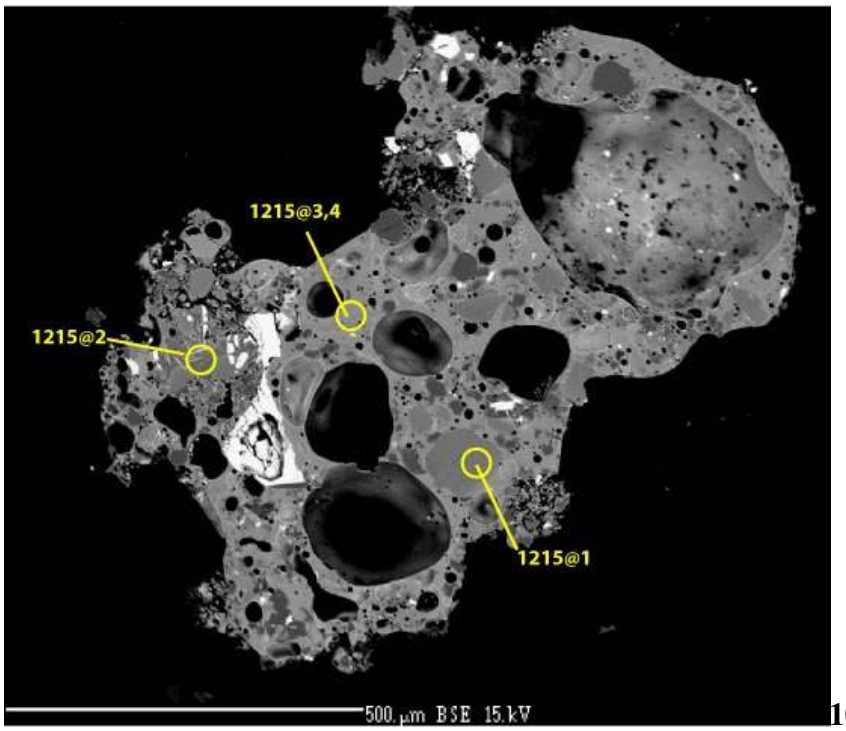

10084agg10

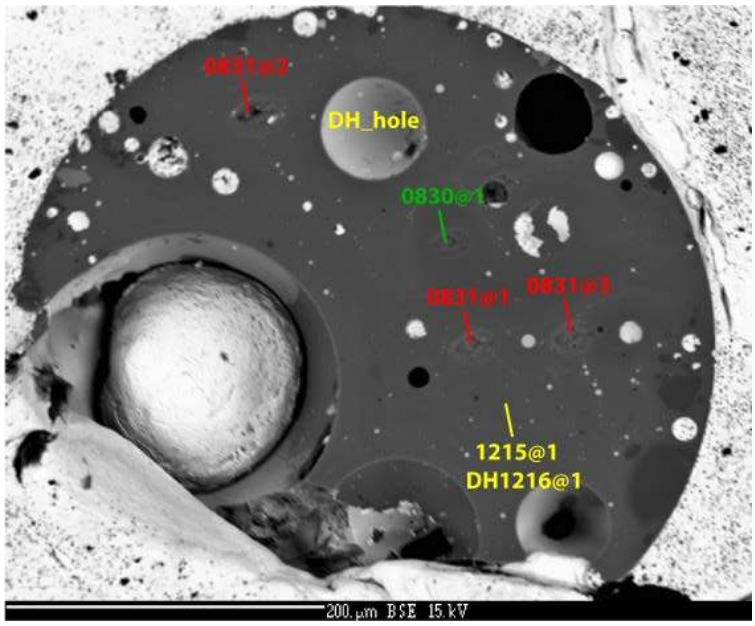

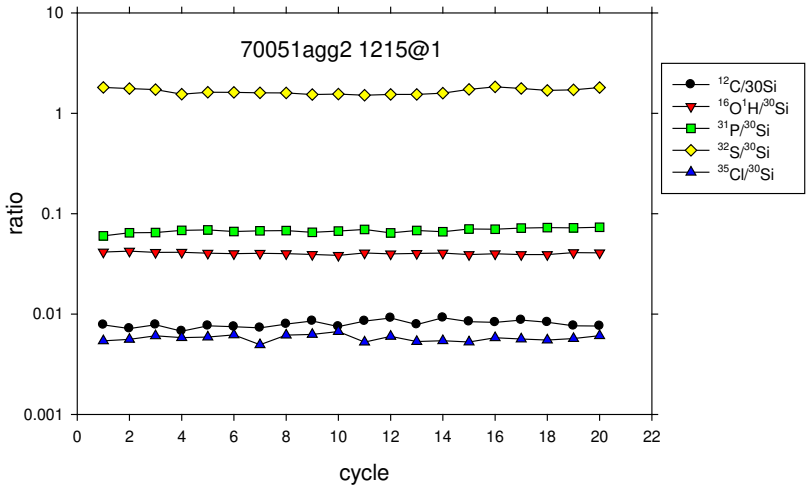

Time lapse for spot 1215@1

70051agg2ir

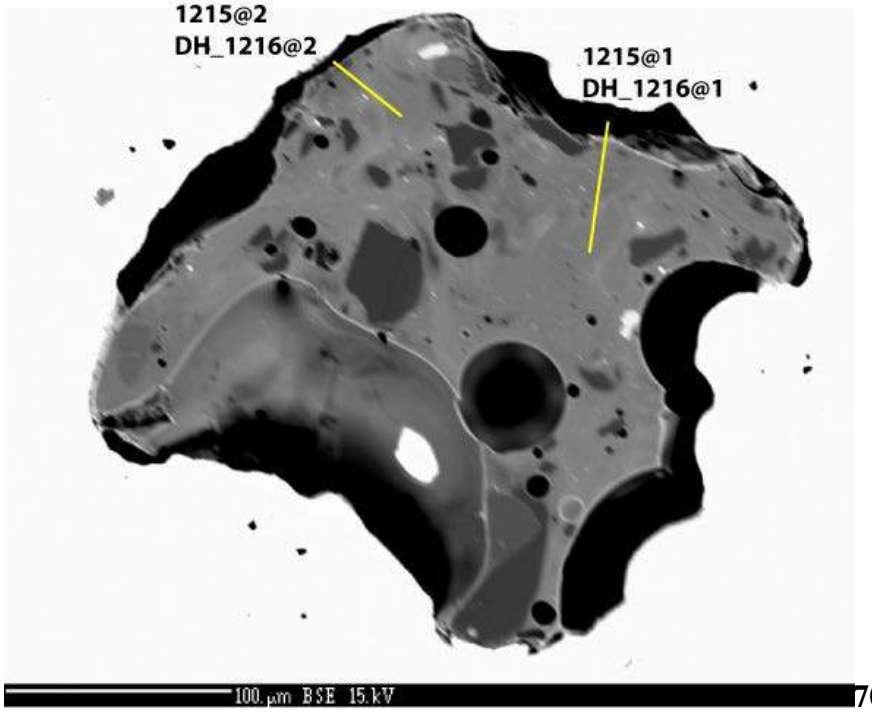

70051agg3ir

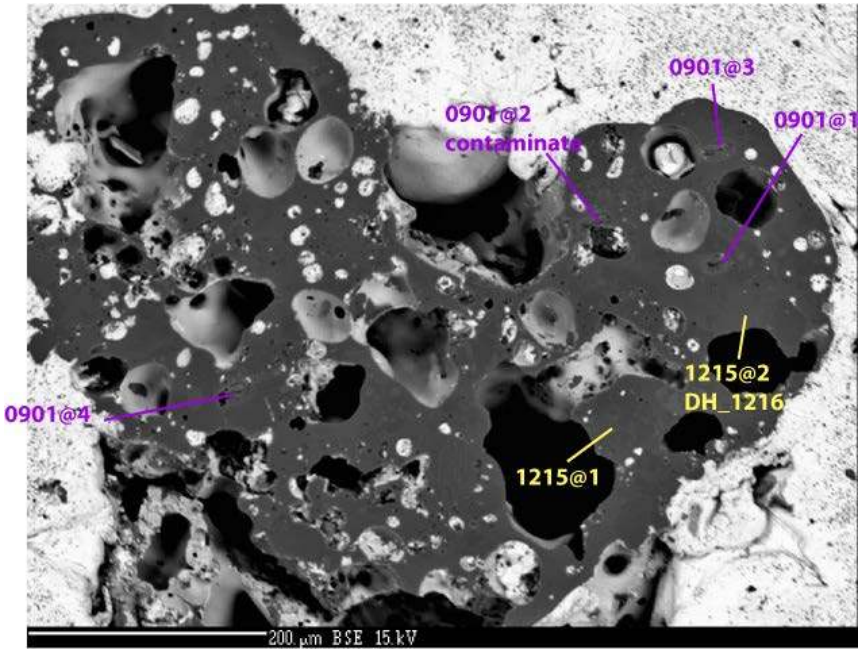

64051 agg3

Supplementary Figure 5. Measured versus modeled D/H values. The modeled D/H assumes all H was derived by solar-wind protons and D was from spallation. The large uncertainties in δD_{model} are due to the uncertainties in H contents.

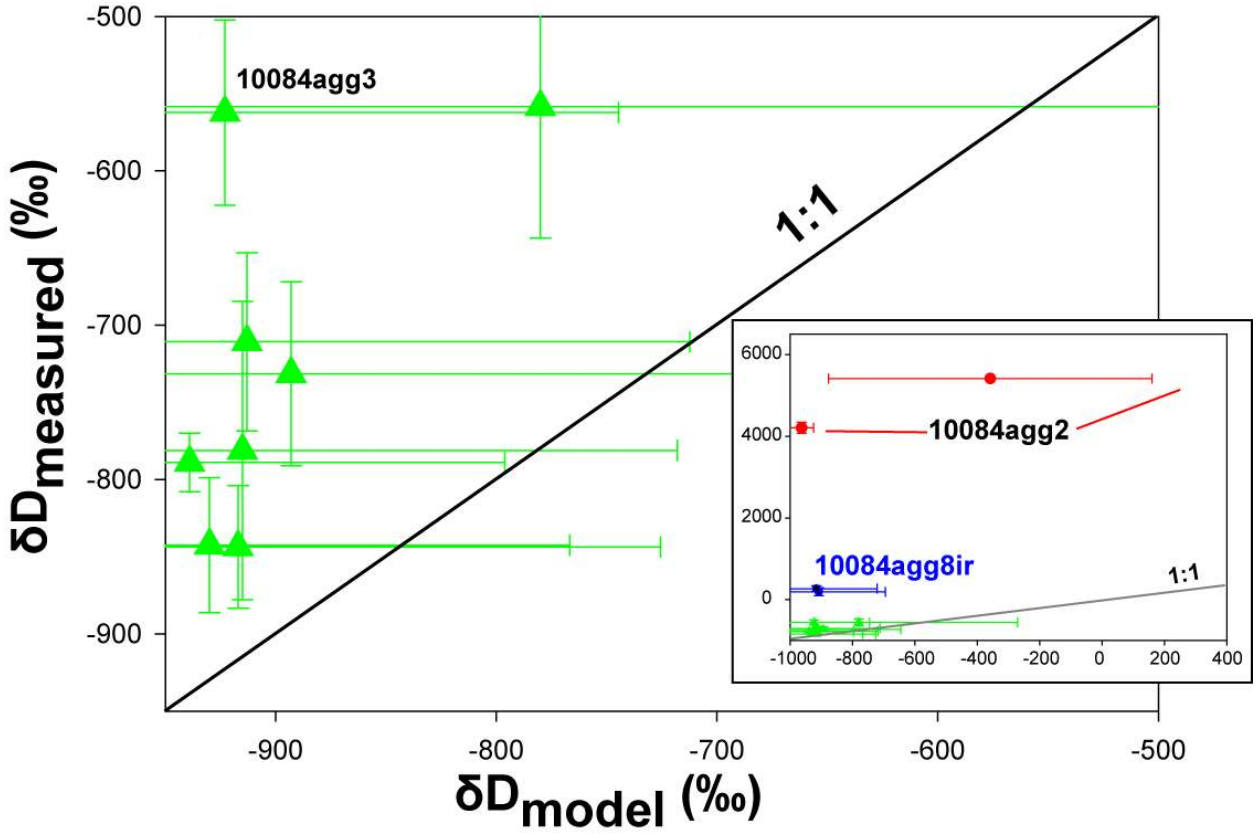

Supplementary Table 1. Composition of agglutinates and their OH contents (in ppmw H_2O).

sample	spot #	H_2O FTIR	H_2O SIMS	2σ	δD (‰)	2σ	P_2O_5	1σ	SiO_2	1σ	TiO_2	1σ	Al_2O_3	1σ	Cr_2O_3	1σ	MgO	1σ	CaO	1σ	MnO	1σ	FeO	1σ	Na_2O	1σ	K_2O	1σ	S	1σ	Total
impact glasses																															
10084impg1			<d.l.		nd		0.29	0.02	42.4	0.2	7.14	0.12	12.8	0.2	0.38	0.02	9.55	0.11	10.9	0.1	0.20	0.02	15.0	0.3	0.44	0.03	0.15	0.03	0.12	0.09	99.5
10084impg2			<d.l.		nd		0.27	0.03	42.2	0.2	7.28	0.14	12.7	0.1	0.39	0.03	9.91	0.09	10.7	0.1	0.21	0.02	15.0	0.3	0.45	0.02	0.14	0.04	0.34	0.46	99.6
70051b1			<d.l.		nd		0.08	0.03	38.4	0.1	9.27	0.17	5.69	0.06	0.68	0.05	14.8	0.1	7.16	0.09	0.28	0.02	22.6	0.2	0.34	0.01	0.06	0.03	0.12	0.15	99.4
64501gg			<d.l.		nd		0.19	0.02	44.5	0.2	0.48	0.08	26.9	0.2	0.11	0.02	7.00	0.14	15.2	0.2	0.07	0.02	5.20	0.16	0.22	0.10	0.06	0.01	0.26	0.28	100.1
agglutinates																															
Apollo 11 soil 10084																															
10084agg1ir	1215@2		187	40			0.23		43.9		2.58		20.3		0.18		7.5		13		0.13		11.5		0.34		0.05		0.01		99.6
10084agg2	0901@1		470	18	4555[2]	95[2]	0.21	0.03	42.1	1.9	6.47	2.2	13.4	2.9	0.29	0.09	9.23	0.71	12.2	0.4	0.22	0	15.0	2.2	0.41	0.08	0.09	0.01	0.43	0.24	100.1
10084agg2	1216_ DH		nd		4206	134																									
10084agg2	0901@2		27	14	5413[2]	687	0.35	0.03	41.0	0.3	10.8	0.3	9.52	0.15	0.32	0.06	6.8	1.3	10.7	0.6	0.25	0.02	19.7	1.4	0.53	0.07	0.17	0.03	0.47	0.46	100.6
10084agg2	0901_ DH@1		nd		1016[2]	32[2]	0.18		45.3		1.91		21.1		0.13		8.2		13.9		0.14		8.66		0.64				0.64		101
10084agg2	1216_ DH@1		nd		1372	142																									
10084agg3	0830@3		121	20			0.22	0.04	43.8	1.4	5.84	0.54	12.1	1.3	0.33	0.04	8.85	0.64	12.2	0.7	0.21	0.03	15.0	0.8	0.34	0.06	0.11	0.01	0.33	0.26	99.2
10084agg3	0830@4		*600*	*18*			0.39		41.2		10.7		9.65		0.44		8.60		11.6		0.23		16.9		0.43				0.25		100.4
10084agg3	0901@2		389	16			0.21	0.06	42.1	0.8	6.70	0.18	14.2	0.4	0.30	0.03	8.20	0.21	12.1	0.5	0.21	0.03	14.8	0.8	0.35	0.06	0.07	0.01	0.68	0.85	99.9
10084agg3	1216@1		316	40																											
10084agg3	1216@2		225	40	-562	60	0.26		42.2		6.63		15.2		0.26		8.09		12.3		0.19		14.3		0.43		0.17		0.13		100
10084agg4n	1215@1		177	40			0.22	0.01	40.7	0.7	7.67	0.2	15.4	1.3	0.31	0.04	7.46	0.59	12.2	0.2	0.19	0	15.1	0.3	0.41	0.03	0.10	0.02	0.10	0.00	99.9
10084agg4n	1215@2		282	40	-789	19	0.28		39.8		8.21		12.7		0.29		8.23		11.6		0.18		18.7		0.38		0.15		0.17		101
10084agg4n	1215@3		246	40	-843	44	0.23		43.2		6.64		9.43		0.36		10.4		12.3		0.23		16.4		0.30		0.09		0.06		99.6
10084agg5ir	0830@2		94	18			0.23		45.3		6.18		9.68		0.54		12.5		12.9		0.20		13.1		0.19				0.00		100.8
10084agg5ir	0830@3		61	16			0.25	0.06	42.0	0.0	8.13	0.04	13.0	1.0	0.27	0.14	7.59	2.08	11.7	0.1	0.23	0.01	17.2	1.2	0.27	0.00			0.19	0.27	100.8
10084agg5ir	0830@3b		293	26																											

10084agg5ir	0830@4		72	14			0.26		41.7		8.00		14.7		0.23		7.50		11.8		0.21		15.3		0.51				0.74		101.0
10084agg5ir	0831@1		48	14			0.25	0.02	42.9	0.8	7.55	0.71	14.6	2.0	0.28	0.09	7.63	0.32	13.1	0.9	0.17	0.1	13.2	3.7	0.57	0.24			0.30	0.26	100.5
10084agg6ir	1215@1	130	161	40	-731	60	0.25	0.07	41.5	0.8	8.09	0.7	12.8	0.3	0.31	0.01	7.95	0.08	11.6	0.2	0.20	0.00	16.8	1.9	0.42	0.03	0.12	0.04	0.13	0.10	100
		170																													
10084agg7	1215@1		83	40			0.20	0.02	42.2	0.3	7.52	0.2	12.7	0.1	0.29	0.00	8.90	0.12	11.6	0.0	0.22	0.00	15.2	0.0	0.52	0.04	0.06	0.03	0.26	0.06	99.6
10084agg7	1215@2		131	40			0.22		41.3		7.70		13.4		0.26		8.59		11.6		0.19		15.3		0.56		0.09		0.20		99.4
10084agg8	1215@1		188	40	191	99	0.20		41.5		9.11		11.3		0.27		8.27		11.6		0.21		16.8		0.49		0.08		0.23		99.9
10084agg8	1215@2		207	40	267	74	0.20	0.01	41.6	0.2	8.08	0.92	12.8	1.5	0.29	0.03	8.49	0.17	11.5	0.2	0.20	0.01	15.9	1.1	0.52	0.05	0.09	0.02	0.22	0.03	99.9
10084agg9	1215@3		47	40			0.54		54.1		1.35		16.3		<d.l.		1.27		8.99		0.17		14.1		1.44		0.75		0.07		99.2
10084agg9	1215@4		219	40			0.23	0.00	43.3	1.3	6.51	0.72	11.5	1.4	0.28	0.06	8.70	1.16	12.2	0.71	0.21	0.03	16.3	1.0	0.38	0.06	0.12	0.09	0.06	0.02	99.7
10084agg10	1215@2		49	40			0.46		53.1		1.94		16.7		0.03		1.82		9.52		0.15		13.9		1.41		0.78		0.12		99.9
10084agg10	1215@4		175	40			0.31		43.8		7.40		10.8		0.28		8.68		11.0		0.21		16.1		0.29		0.31		0.25		99.5
Apollo 17 soil 70051																															
70051agg2ir	0830@1		87	14			0.11		49.8		3.17		3.44		0.46		15.0		15.0		0.18		13.0		0.16						100.3
70051agg2ir	0831@1	150	171	14			0.14	0.03	38.9	0.8	6.84	0.32	14.0	0.6	0.41	0.06	10.1	0.4	10.8	0.3	0.19	0.02	17.8	0.5	0.22	0.03	0.06	0.00	0.46	0.44	99.9
70051agg2ir	0831@2		161	16			0.12	0.01	38.5	0.2	7.02	0.15	13.3	0.6	0.41	0.01	10.4	0.3	10.7	0.3	0.20	0.01	18.3	0.3	0.20	0.04			0.52	0.67	99.6
70051agg2ir	0831@3		154	16			*0.14*		*44.0*		*5.05*		*10.5*		*0.52*		*11.9*		*14.1*		*0.17*		*13.2*		*0.16*				*0.61*		*100.4*
70051agg2ir	1215@1	120	200	40	-711	58	0.15	0.03	38.2	0.4	6.89	0.16	13.9	0.2	0.42	0.05	10.0	0.23	11.0	0.1	0.19	0.02	18.3	0.7	0.22	0.02	<d.l.	0.03	0.40	0.41	99.7
70051agg3ir	1215@1	90	209	40	-844	40	0.19		41.3		7.30		12.0		0.36		9.43		13.5		0.22		15.3		0.39		<d.l.		0.08		100
70051agg3ir	1215@2	70	203	40	-781	97	0.15		40.6		8.12		12.4		0.40		9.94		11.3		0.22		16.4		0.38		0.06		<d.l.		100.0
Apollo 16 soil 64501																															
64501agg3	0901@3		203	16			0.23	0.01	43.5	0.9	0.92	0.14	27.0	1.2	0.11	0.02	7.38	1.18	15.5	0.4	0.08	0.03	5.25	0.53	0.40	0.07			0.23	0.12	100.3
64501agg3	0901@4		269	50			0.23	0.00	44.2	0.4	0.30	0.26	35.4	0.2			0.10	0.06	18.9	0.4	<d.l.		0.23	0.01	0.60	0.22			0.44	0.27	100.5
64501agg3	1215@2		79	40	-558	85	0.17		44.2		0.14		27.7		0.06		6.55		16.0		0.07		4.15		0.47				<d.l.		99.5
Mineral fragments in agglutinates[3]																															
10084agg1ir	1215@1	pl	<d.l.				0.29		43.4		<d.l.		36.2		<d.l.		0.05		20.0		<d.l.		0.19		0.36		<d.l.		<d.l.		100
10084agg3	0830@1	pl	*43*	*14*			0.22	0.03	44.4	0.3	0.42	0.18	30.5	0.9	0.05	0.02	3.68	0.59	17.4	0.3	<d.l.		3.17	0.48	0.47	0.03			0.13	0.24	100.4

	DH_plag@1				*2018*	*351*																							
10084agg5ir	0830@1	px	<d.l.				0.19	0.07	47.9	0.6	4.19	0.46	4.50	0.68	0.78	0.03	14.8	0.0	16.5	0.3	0.24	0.02	10.9	0.2	0.12	0.01		0.16	0.22	100.3
10084agg8	1215@3	pl	*15*	*40*	*952*	*208*	0.22	0.01	43.8	0.0	0.07	0.01	35.7	0.1			0.17	0.02	19.8	0.0	<d.l.		0.37	0.10	0.35	0.02	<d.l.	0.08	0.05	100.6
10084agg9	1215@2	px	<d.l.				0.12		51.7		0.87		1.04		0.27		18.7		6.21		0.37		21.8		<d.l.		<d.l.	<d.l.		101.1
10084agg10	1215@1	px	<d.l.				0.23	0.01	48.5	0.6	3.34	0.2	3.89	0.50	0.74	0.11	14.9	0.8	17.9	0.7	0.19	0.01	10.4	0.28	0.11	0.02	<d.l.	<d.l.		100.4
64501agg3	0901@1	ol	*46*	*14*			0.09		38.8		0.37		1.80		0.05		36.1		1.11		0.20		22.7		<d.l.			<d.l.		101.2
64501agg3	1215@1	px	<d.l.				0.16		44.0		0.44		20.9		0.12		11.9		11.8		0.15		13.0		0.35			0.24		103.1

[1]OH contents from FTIR were calculated using the OH band height at ~2350 cm-1 and a molar absorption coefficient of basaltic glass (Danyushevsky et al.[2]).

The 2σ uncertainties for SIMS measurements are based on repeated analyses of standards, fitting errors, and counting statistics. Italic numbers indicate possible terrestrial contaminations in the H abundances by SIMS because their vicinities to H hot spots (contaminates). The 1σ uncertainties for oxides are standard deviation of > 3 analyses near the same spots. d. l.: detection limit; nd, not determined.

[2] Errors of these D/H measurements are only from counting statistics.

[3] These D/H measurements on mineral fragments contain larger uncertainties than those from counting statistics owing to the low H contents in these minerals. pl: plagioclase; px: pyroxene; ol: olivine.